High Power Laser Science and Engineering, (2023), Vol. 11, e30, 10 pages.
doi:10.1017/hpl.2023.10

HIGH POWER LASER SCIENCE AND ENGINEERING

RESEARCH ARTICLE

Post-compression of high-energy, sub-picosecond laser pulses

P.-G. Bleotu[1,2,3], J. Wheeler[4,5], S. Yu. Mironov[6], V. Ginzburg[6], M. Masruri[3], A. Naziru[2,3], R. Secareanu[3], D. Ursescu[2,3], F. Perez[1], J. De Sousa[1], D. Badarau[1], E. Veuillot[1], P. Audebert[1], E. Khazanov[6], and G. Mourou[4]

[1] *LULI-CNRS, CEA, Universite Sorbonne, Ecole Polytechnique, Institut Polytechnique de Paris, Palaiseau CEDEX, France*

[2] *Doctoral School of Physics, University of Bucharest, Bucharest-Magurele, Romania*

[3] *Horia Hulubei National Institute for R&D in Physics and Nuclear Engineering (IFIN-HH), Magurele, Romania*

[4] *IZEST, Ecole Polytechnique, Institut Polytechnique de Paris, Palaiseau CEDEX, France*

[5] *Independent Researcher, Bourg-La-Reine, France*

[6] *Federal Research Center Institute of Applied Physics of the Russian Academy of Sciences (IAP RAS), Nizhny Novgorod, Russia*

(Received 11 November 2022; revised 11 January 2023; accepted 3 February 2023)

Abstract

The post-compression technique based on self-phase modulation of high-energy pulses leads to an increase in achievable peak power and intensity. Typically, the pulses considered in experiments have been less than 100 fs in duration. Here, the method is applied to the ELFIE laser system at the LULI facility, for a pulse of 7 J energy and an initial measured duration of 350 fs. A 5-mm-thick fused silica window and a 2 mm cyclic-olefin polymer were used as optical nonlinear materials. The 9 cm diameter beam was spectrally broadened to a bandwidth corresponding to 124 fs Fourier-limited pulse duration, and then it was partly post-compressed to 200 fs. After measuring the spatial spectra of the beam fluence, a uniform gain factor of 4 increase in the fluctuations over the studied range of frequencies is observed, due to small-scale self-focusing.

Keywords: high-power laser; nonlinear pulse interaction; post-compression; self-phase modulation

1. Introduction

The efficient compression of the available laser energy into an ever shorter pulse duration is an important tool in creating ultra-high-peak intensity laser pulses. Few-cycle, and even single-cycle, laser systems are routinely available at table-top (mJ and below) scale energy levels that have opened up a wide range of applications in strong-field physics, including time-resolved imaging and pump-probe studies. High-power, few-cycle laser pulses at the level of multiple Joules are considered an important next step in the efficient control over strong-field, laser–plasma processes to extend into the next level of practical applications related to particle acceleration and nuclear photonics[1]. While chirped pulse amplification (CPA)[2–4] has enabled the advancement of ever-growing energy levels into short pulse laser systems, the limitations in bandwidth for the amplifiers and stretcher–compressor technology has historically limited high-energy pulses from reaching their shortest possible duration, as defined by the carrier wavelength ($\tau_p \sim \lambda/c$). The post-compression techniques utilized in low-energy laser systems are typically based on photonic crystal fibers[5], hollow-core fiber waveguides[6] and multi-pass cells[7]. Unfortunately, none of these approaches are well-suited even for sub-J laser pulses[8].

In contrast, the thin film compressor (TFC), or compression after compressor approach (CAfCA), is demonstrated for the post-compression of just such large-scale CPA laser systems[9–11]. The basic principle relies upon current concepts of post-compression where a nonlinear process such as self-phase modulation (SPM) introduces additional spectral bandwidth, and then the phase of the pulse must be controlled over the entire bandwidth to maintain the desired pulse duration. For the TFC, it is sufficient to use a transparent film of appropriate thickness interacting across the full aperture of the freely propagating flat-top,

Correspondence to: P.-G. Bleotu, Doctoral School of Physics, University of Bucharest, 077125 Bucharest-Magurele, Romania. Email: gabriel.bleotu@eli-np.ro

high-energy pulse within its transport from the final optical compressor to the final target. The intensity of these pulses – of the order of TW/cm^2 – is sufficient to drive nonlinear spectral broadening through SPM that arises from the time-dependence of the material index of refraction, $n(t) = n_0 + n_2 I(t)$, due to the influence of the laser intensity, $I(t)$. Here, n_0 is the linear part of the refractive index and n_2 is the nonlinear refractive index. Due to the nature of the nonlinear laser–material interaction, the group delay dispersion (GDD) compensation required is primarily of second-order spectral phase correction. The dispersion correction factor (α) meant to optimize the GDD of the resultant pulse is most efficiently performed using optical elements such as chirped mirrors (CMs). One principle benefit of this configuration is the low energy losses during the SPM interaction, which allow for an efficiency over 90% and for several stages to compress the pulse to the desired duration. The low energy losses permit the option to employ multiple stages to decrease the pulse to the desired duration[12].

The SPM process is the effect of the rapid change in the material index of refraction associated with the fast electric field oscillations of the intense laser pulses. The bandwidth modifications are easier to observe on laser systems with a shorter initial pulse. Thus, the compression technique has been studied at the TW-scale at several of these laser systems, including CETAL, ALLS, PEARL, ELI-NP and CoReLS[13–19], demonstrating up to five-fold pulse compression[20], and even six-fold[21]. The technique was applied in producing betatron radiation from laser wakefield acceleration (LWFA)[22], and the method is now being implemented on PW-scale laser systems[23,24]. A successful demonstration of the TFC on a laser system with an initial duration greater than 100 fs has great potential as an economical upgrade to existing picosecond-scale, high-energy laser systems, such as PETAL, OMEGA-EP and Vulcan.

To date, post-compression has been tested with long pulses at only tens of mJ[25,26] but preliminary numerical simulations for post-compressing PETAL laser parameters of 1 kJ, 0.5 ps and 200 mm diameter beam predict the ability to reach approximately 100 fs and suggest the peak power could be increased by nearly four times with a single-stage compressor[13].

In addition to existing laser installations, there is the possibility to apply the post-compression to novel designs. The need for an efficient high peak and average power laser driver is crucial for laser–plasma processes to be extended beyond discovery science and be put into practical application. A proposed solution for an industrial-scale, high-energy laser operating at more than or equal to 100 kHz employs a fiber chirped pulse amplification (FCPA) system. The small energy of a single fiber amplifier can be overcome by coherently combining several such amplifiers in parallel. This laser architecture concept is also known as the coherent amplification network (CAN). It has been introduced for driving particle acceleration[27,28] and systems with up to 61 fibers are under further development[29,30]. While efficiently producing pulses at a high repetition rate, the bandwidth limitation of a fiber-based amplifier places the minimum pulse duration near 300 fs and would require a post-compressor to reach the few-cycle pulse regime. Therefore, an FCPA laser system will likely benefit from highly efficient post-compression stages in order to reach a high compression factor. The development of an efficient and expandable CAN laser system based on fiber laser technology gives access to an economical and flexible tool capable of meeting the requirements of a wide range of applications, including the ability to drive the multiple stages of acceleration within a laser accelerator facility[31].

The output bandwidth of the SPM process ($\Delta\omega_{\mathrm{spm}}$) is proportional to the nonlinearity accumulated by the pulse in traversing the material[11]. This process is quantified using the B-integral parameter, $B_{\mathrm{int}} = (2\pi/\lambda) \cdot I_{\mathrm{o}} \cdot n_2 \ell_{\mathrm{i}}$, which takes into consideration the laser parameters of average peak intensity I_{o}, the wavelength λ and the interaction distance ℓ_{i}, with a material of nonlinearity n_2. Due to the typical positive material dispersion ($k_2 > 0$, where k_2 is the group velocity dispersion), the expected broadening is reduced due to the decreasing intensity as the pulse stretches in time. Thus, the dispersion is dependent on the initial pulse duration with an increased sensitivity for a shorter pulse with a broader initial spectrum. These dispersion effects can be summarized in the term $D = \ell_{\mathrm{i}} k_2 / \left(\tau_{\mathrm{p}}\right)^2$, which considers again the interaction length, material dispersion and initial pulse duration. The model for the dependence on B and D of the spectral broadening relative to the original pulse spectrum is related to $F_\omega \equiv (\Delta\omega_{\mathrm{spm}}/\Delta\omega) = 1 + g_\omega B_{\mathrm{int}}(1 - h_\omega\sqrt{D})$. Here, g_ω and h_ω are fit parameters that were determined from simulations of SPM spectral responses under appropriate conditions to have values of $g_\omega \sim 0.91$ and $h_\omega \sim 1.5$.

An advantage of beginning from long Fourier transform-limited (FL) pulses is the extremely weak influence of the linear dispersion of the medium. As the parameter D is inversely proportional to the square of τ_{p}, reducing D improves the efficiency of the post-compression for a given B_{int}. An increase in the initial pulse duration also increases the maximum possible factor of compression in time, because the shortest duration for the pulse remains fixed by the optical cycle. Thus, employing multiple stages of compression can make possible the attaining of very high compression factors for these long pulses.

The dispersion management requires a high GDD, as the phase correction is proportional to the square of τ_{p}. As exemplification, a 150 fs ($\Delta\lambda \sim 11$ nm) pulse is only modified by GDD of the order of approximately 2.3×10^4 fs^2 and a pulse of 350 fs ($\Delta\lambda \sim 5$ nm) requires GDD of approximately 1.2×10^5 fs^2 to induce a significant influence on the pulse duration.

https://doi.org/10.1017/hpl.2023.10 Published online by Cambridge University Press

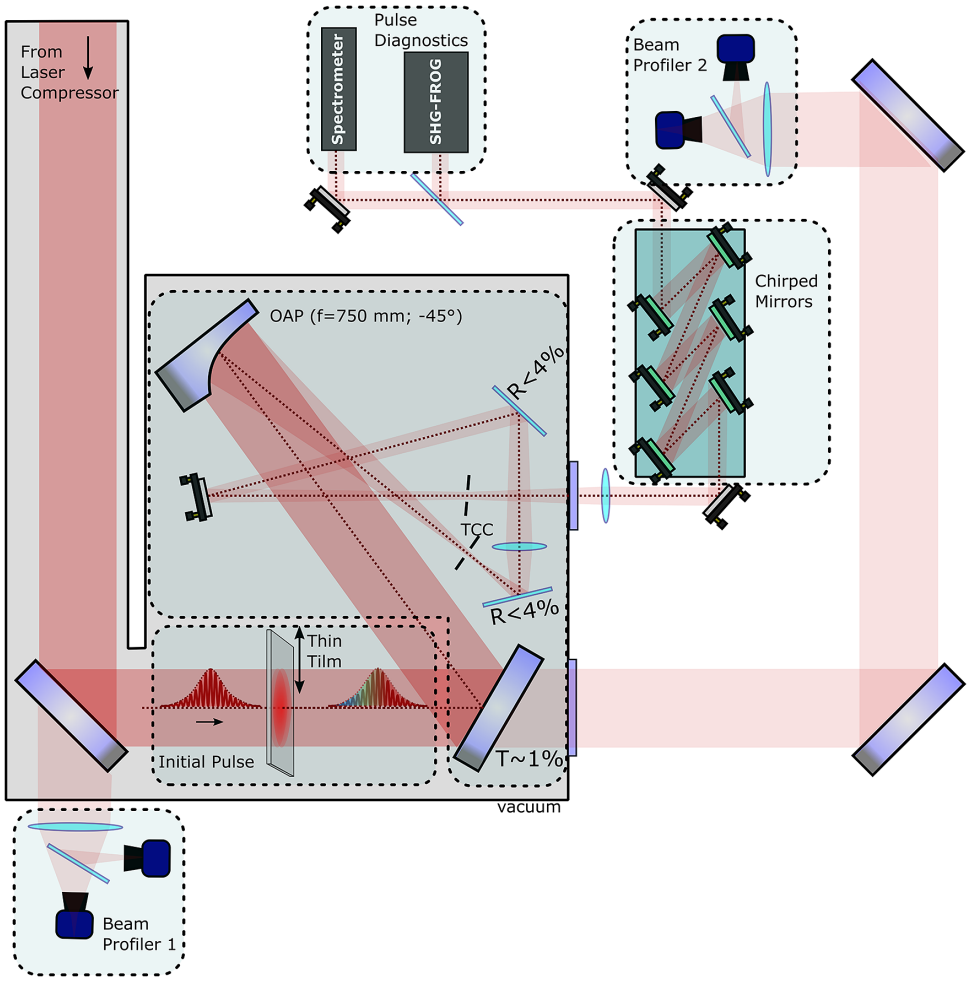

Figure 1. The experimental setup for a demonstration of the post-compressor within the ELFIE interaction chamber. OAP is the off-axis parabolic mirror and TCC is its focus position.

This is highlighted within this experiment (see Figure 1, ELFIE laser, 350 fs) where the dispersion introduced by the diagnostic beam transport – including a set of CMs (–6000 fs^2) – is not significant enough to show effects on the initial pulse, while the spectrally broadened pulse reaches bandwidths that are sensitive to the dispersion. For an existing beamline, any change in the pulse duration will need to consider the limitations of the subsequent optics in effectively transporting the modified pulse. Again, the use of multiple compression stages with each stage designed to accommodate the increasing bandwidth/decreasing FL pulse duration and the corresponding increase in pulse intensity will likely be required in order to reach the highest pulse compression factors.

As the peak power of the pulse exceeds the critical power $P_{cr} = 3.79\lambda^2/(8\pi\, n_0 n_2)$ (P_{cr} ~4.5 MW for fused silica (FS)), the intense pulses with super-Gaussian modes are susceptible to multi-filamentation through the modulational instability initiated by noise in the beam profile[32]. The process of spatial harmonic instability starts at a distance inside a nonlinear medium, where the nonlinear phase (or B-integral) exceeds unity. Pulses where $P \gg P_{cr}$ eventually break up into multiple filaments during propagation through a medium of sufficient length[33]. The choice in thin film (TF) is to optimize the material interaction length that maximizes the spectral response while introducing minimal adverse effects on the spatial profile and pulse wavefront. The lower peak intensity of longer pulses requires more material to attain significant spectral broadening, which can be more economical to manufacture at the optical transmitted wavefront quality desired to minimize effects on the beam.

Therefore, the evolution of the small-scale self-focusing (SSSF) and multi-filamentation process that develops due to modulation instabilities in the beam must be considered in order to understand how it will be detected in measurements of the near-field profile. An important aspect is controlling the influence of the SPM process on the beam profile quality[34–36] and the small-scale filamentation and beam break-up. Unmitigated development within the profile eventually leads to damage of the nonlinear material or subsequent optics and loss of pulse energy, and the aberrations diminish the achievable focus quality.

https://doi.org/10.1017/hpl.2023.10 Published online by Cambridge University Press

In this paper, measurements of spectral broadening and the influence of the SPM process for a sub-picosecond high-energy laser pulse interacting with glass and polymer materials are reported. Section 2 describes the experimental configuration implemented during the campaign at the ELFIE laser facility. Section 3 examines three aspects of the laser pulse following the nonlinear interaction: (1) the effect on the laser focus; (2) the measured spectral and the temporal responses are compared with the expectation from simulations; (3) the relative gain in the spatial modulation instabilities of post-compressed laser pulses. Section 4 summarizes the implications of the results in planning future experiments.

2. Methods

2.1. Laser system

The ELFIE laser facility is based on a CPA laser architecture starting from a Ti:sapphire front-end followed by mixed silicate/phosphate glass amplifiers. The laser beam is compressed under vacuum to a duration of roughly 350 fs at wavelength $\lambda = 1.057$ μm. The repetition rate is one shot every 20 minutes at full energy of 7 J per shot for this experimental campaign. The beam is typically 11.5 cm in diameter after the amplification chain, but a 7.0 cm diameter apodizer was placed before the final amplifier in order to improve the uniformity of the useful beam profile. Therefore, the energy of the pulse is reduced by a factor of approximately 0.74 with respect to the typically measured one.

For this campaign, the laser pulse energy is measured to be $\mathcal{E}_L \sim 6.5 \pm 0.8$ J within the full diameter beam and correcting for the apodizer gives a typical interaction energy of $\mathcal{E}_L \sim 4.8 \pm 0.7$ J. The beam diameter is estimated from beam profile images (BP2 in Figure 1) to be of the order of 9 cm after propagating to the point of interaction with the film.

Just as with the shot-to-shot variation of the pulse energy, the duration has been noticed to fluctuate in the temporal measurements but stayed between 330 and 380 fs with the mean value of 350 fs corresponding to a factor of 1.1 times the FL pulse duration after the compressor. Achieving this duration at full power did require adjusting the optical grating separation distance by approximately 1.25 mm relative to the optimum measured under the low-energy alignment conditions. The compressor position is best optimized by observing the nonlinear spectral broadening and maximizing its spread (see Section 3.2). The peak intensity among the shots is estimated to fall between $I_o \sim 0.2$ and 0.3 TW/cm^2, with the shots considered in the following analysis having an average peak intensity of $I_o \sim 0.23$ TW/cm^2.

2.2. Post-compression test configuration

The experimental setup is depicted in Figure 1. A beam profiler (BP1) monitors the leakage passing through the last turning mirror before entering the interaction chamber. The TF (technically an optical window at the thickness required for these intensities) is mounted to a motorized stage installed shortly after the entrance to the interaction vacuum chamber within the ELFIE installation. The mount enables the TF to be inserted or removed without requiring the chamber to be opened.

Table 1. Thin film material properties at $\lambda_L = 800$ nm.

Material	FS	COP
ℓ_i [mm]	5	2
n_0	1.4497	1.5201
n_2 [cm^2/W]	2.5×10^{-16}[37]	5.8×10^{-16}[38]
k_2 [fs^2/mm]	16.994	52.217

Two types of materials are considered: FS glass and cyclic-olefin polymer (COP, known as Zeonor). The thickness of the nonlinear plates is 5 mm for FS and 2 mm for COP. Their relevant optical properties are summarized in Table 1. The FS sample is a laser-grade optical window, while the COP sample is an optical slide made for the manufacture of optical chips in microfluidic studies and is not of optical laser quality (i.e., wavefront, roughness). This difference becomes obvious in the results but information on the polymer sample is included to compare the nonlinear response for its potential application within laser-quality optical samples.

After the initial laser pulse interaction with the TF element, the objective is to sample the focus, monitor the beam spatial mode quality for film damage and record the pulse spectrum and its duration. Care must be taken in the attenuation of the pulse energy to avoid contributing additional nonlinear effects in the subsequent optical elements. However, at the expected pulse duration ($\tau_p > 100$ fs), the influence of additional dispersion due to the transport optics is not as constraining as in the case of ultrashort pulses ($\tau_p < 100$ fs). The first mirror after the nonlinear window is a partially reflecting mirror (reflectance 99%; transmittance 1%). The transmitted fraction of the beam exits the chamber through a vacuum window (BK7, 25 mm) before traveling 3 m to a second beam profiler (BP2) based on two 8-bit cameras for measuring the focus quality and a near-field image at the plane of the TF.

The reflected fraction of the beam continues to the standard off-axis parabola (OAP) of the interaction chamber, which is employed as the first of a three-element reducing telescope. An uncoated wedge is placed at a sufficient distance, after the target chamber center (TCC) focus of the OAP, to attenuate the beam (reflectance ~ 0.006 for p-pol light) without creating damage to the optical components and to avoid potential damage on subsequent optics at the reduced beam diameter. Half of this wedge has a silver coating and is motorized so that this portion can be moved into the beam during alignment mode at low energy. A lens ($f = 30$ cm) is placed at a distance slightly beyond 30 cm

https://doi.org/10.1017/hpl.2023.10 Published online by Cambridge University Press

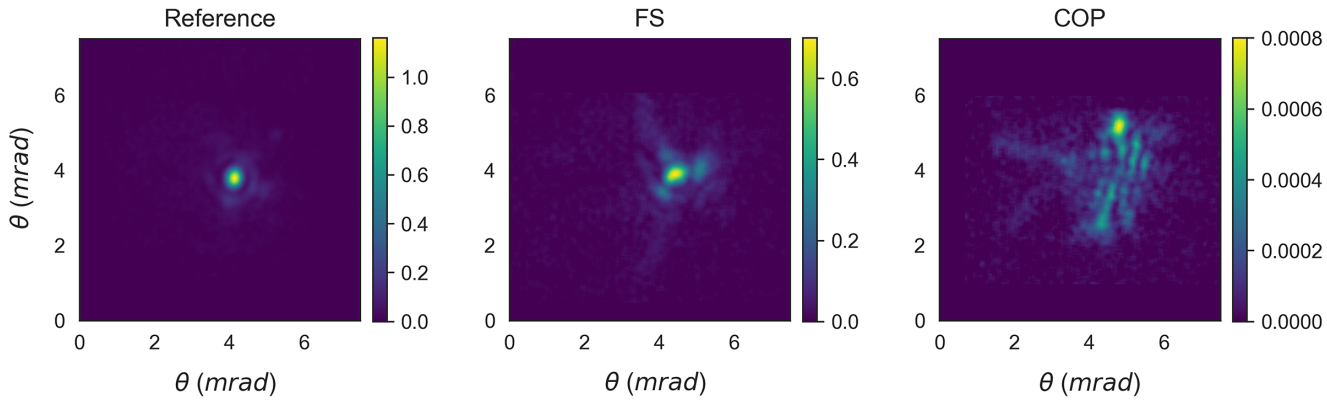

Figure 2. Images of the focused laser beam after traversing no material (left), 5 mm fused silica glass (center) and 2 mm COP (right).

after the TCC focus to avoid damaging the optics but before the beam expands beyond its 75 mm diameter. Thus, the expected beam diameter is 45 mm.

The low-energy pulse passes through a 7-mm-thick MgF_2 window to be re-collimated by a third lens to a beam of approximately 1 cm diameter before continuing to the optical diagnostic table on 25 mm aperture optics.

A series of six negative-dispersion mirrors (UFI HD65; design bandwidth 1010–1070 nm) are installed that can each provide a phase correction of -1000 fs^2 for a total GDD contribution of -6000 fs^2. This is an insufficient value to see an influence on a 350 fs pulse, but is expected to partially re-compress the pulse with a broader spectrum. The diagnostics available for characterizing the pulse consist of an imaging spectrometer, an autocorrelator (AC) and a second harmonic generation–frequency resolved optical gating (SHG-FROG). While the spectrograms of the SHG-FROG were useful for real-time feedback during the experimental campaign, the low signal at the input port of the device meant the reconstructed error was too large to report those results here.

3. Results

The modified properties of the laser pulse are measured after the interaction with the nonlinear substrate. The three primary aspects reported here are the effect on the focus, the spectral/temporal response and the small-scale features that develop within the beam spatial profile.

3.1. Focus quality of the optical components

The quality of the optical components, including in particular the transmitted wavefront distortion, plays an important role in the far-field (FF) modifications of the laser beam. In Figure 2, a comparison of the focal spots measured in the BP2 profile is presented using the reference beam without material, after 5 mm FS and after 2 mm COP. The low optical quality of the COP material is obvious in the deterioration of the focal spot in Figure 2, right-hand side.

A suitable implementation of this material with mm-scale thickness will require higher laser quality samples to be used. The beam can still be brought to a focal spot comparable to the original reference if a better laser quality substrate, such as an FS sample (despite being thicker), is used. Even if the FF image is degraded, a deformable mirror is likely capable of compensating for the wavefront deformation, as shown in Ref. [39]. Due to the low optical quality of this sample of COP, the wavefront is too disrupted for correction or pulse characterization, beyond simple spectrometer measurements.

3.2. Spectral response

The effects of the COP on the beam adversely impact the pulse duration measurements of the resultant pulse, and so only the spectrum produced by COP is given for comparison with FS. Results of simulations of the spectrum broadening and temporal post-compression for the ELFIE laser pulse interacting with 5 mm FS are shown in Figure 3. The temporal shape of the laser pulse is obtained with the help of the inverse Fourier transform from the measured spectral intensity distribution (see Figures 3(e) and 3(f)). The initial condition assumes that the pulse on the entrance surface has the FL duration of $T_{in} = 300$ fs and a flat-top beam diameter of 9 cm. Taking into account that the pulse energy can vary from shot to shot, a range of energies up to 10 J is considered in the calculations.

Figure 3(a) describes the simulated spectral broadening as a function of the energy after the pulse travels through the FS plate. In accordance with this figure, more energy in the initial pulse corresponds to higher nonlinear phase accumulation and, as a consequence, wider spectral broadening. The temporal intensity distributions of the compressed laser pulse obtained after spectral phase correction with the CM having the GDD parameter $\alpha_{CM} = -6000$ fs^2 (the value corresponds to the experimental conditions) are given in Figure 3(b), as a function of pulse energy. The FL pulses are presented in Figure 3(c). The pulse durations, at the fixed and optimal values of GDD, are presented in Figure 3(d).

https://doi.org/10.1017/hpl.2023.10 Published online by Cambridge University Press

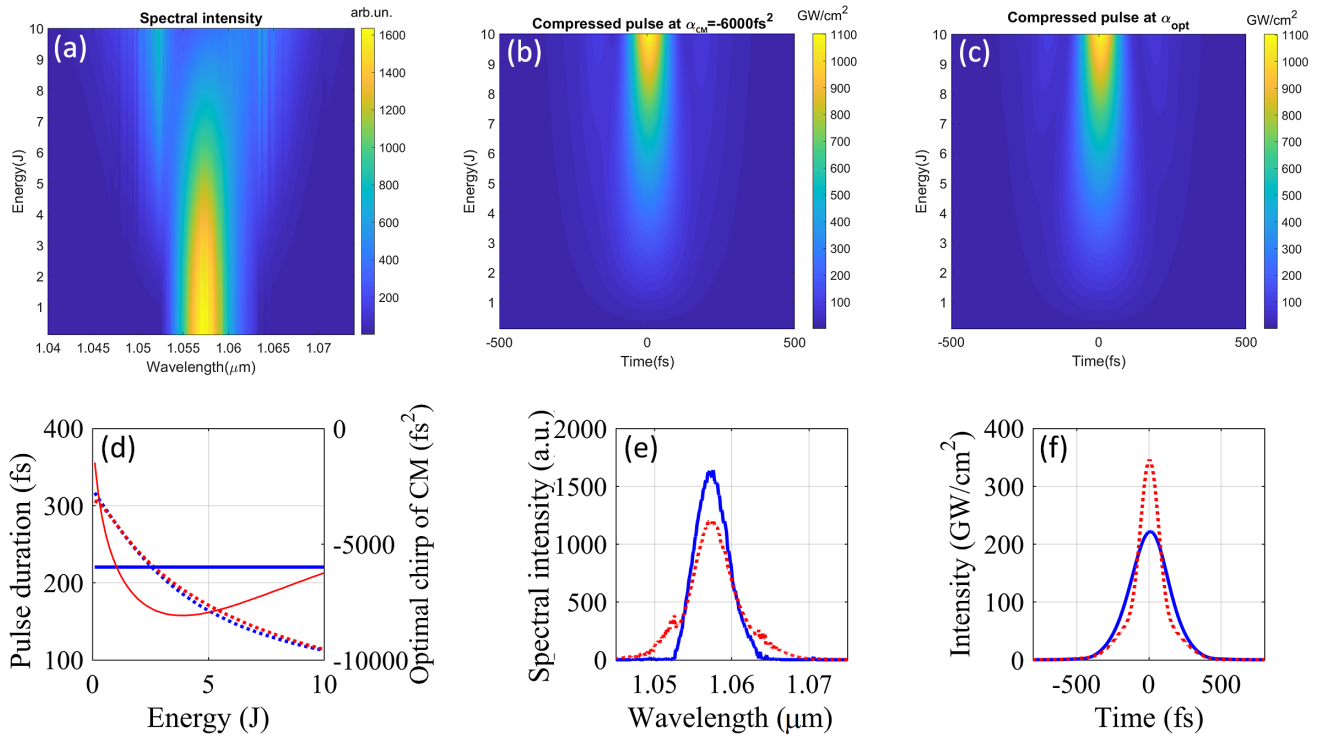

Figure 3. Simulations of spectral broadening for pulses interacting with 5 mm fused silica, based on ELFIE laser parameters. The top row (a)–(c) considers the resultant spectra and pulse temporal shape for the compressed pulse as a function of the input pulse energy. Middle column: pulse shape for the dispersion compensation α_{CM}= –6000 fs^2. Right-hand column: FL pulse shapes. In (d), the dotted red and blue lines describe the duration of the FL compressed pulse (red solid) and fixed $\alpha_{CM} = -6000$ fs^2 (blue solid), respectively. (e) The measured input spectrum (blue) and output spectrum (dotted red) for 4.8 J pulse energy. (f) The corresponding reconstructed shape for input (300 fs, blue) and output (170 fs, dotted red) pulse.

The optimal value is chosen as the highest peak intensity of the compressed pulse and not the minimum pulse duration. It can be seen that the difference between the two cases is insignificant. It means that for wide input pulse energies (one order of magnitude) the fixed set of CMs is enough for obtaining pulse shortening in the experiments. The spectrum intensity distribution and the compressed temporal shape obtained at a pulse energy of 4.8 J are presented in Figures 3(e) and 3(f), respectively. For this case, the duration of the compressed pulse is similar to the value obtained in the experiments (see Figure 4).

The spectral amplitudes recorded during the experimental campaign by the imaging spectrometer are shown in Figure 4. The original laser spectrum sampled after the final amplifier (blue dashed line) is compared with the broadening that occurs when no material (Figure 4(a), red line), FS (Figure 4(b), green line) and COP (Figure 4(c), orange line) are present in the beam during the same shot. Throughout Figure 4, the central wavelength of the laser system is $\lambda =$ 1057.5 nm and the reference spectrum maintains a full width at half maximum (FWHM) bandwidth $\Delta\lambda_{ref} = 5.4 \pm 0.3$ nm, sufficient to support a Fourier-limited pulse of approximately 300 fs pulse duration. In Figure 4(a), with no material interaction, the lack of broadening demonstrates that no contribution to the SPM occurs during the beam transport and measurement. The specific shot depicted in Figure 4(d) shows an autocorrelation measurement for a pulse duration of 340 ± 10 fs. The energy measured for this specific shot was $\mathcal{E}_L \sim 4.2$ J. For the case of the specific FS shot highlighted in Figure 4(b), the energy is measured to be slightly greater at $\mathcal{E}_L \sim 4.8$ J, and the bandwidth expands to $\Delta\lambda_{FS} = 13.3$ nm, which is capable of supporting a pulse duration of 124 fs.

For the laser shot interacting with the COP film in Figure 4(c), the pulse energy is lower at $\mathcal{E}_L \sim 3.9$ J. When considering the spectrum for the COP, the FWHM bandwidth broadens to $\Delta\lambda_{COP} = 12.4$ nm, which supports the shortest pulse duration of 132 fs.

From this data, the measured ratio for the spectral increase for FS is $F_\omega^{FS} = 2.66$. The ratio F_ω^{FS} can be compared with the models derived by Khazanov *et al.*[11] for the expected broadening by considering that $B_{int} \sim 1.78$ and $D \sim 0.00078$ give an expected factor of $F_\omega^{FS} = 2.6$.

Figures 4(d) and 4(e) show the AC measurement with no material and after the interaction with the FS window along with the set of CMs. Assuming a Gaussian pulse temporal profile, the AC fit gives an initial reference pulse duration of 340 fs and a reduced pulse duration of 200 fs after the introduction of the FS. This suggests a chirp due to GDD of approximately 3000 fs^2. The difference between the calculated optimum compensation for the SPM alone ($\alpha_{opt} \sim 8000$ fs^2) and the CMs provided is –2000 fs^2. The

https://doi.org/10.1017/hpl.2023.10 Published online by Cambridge University Press

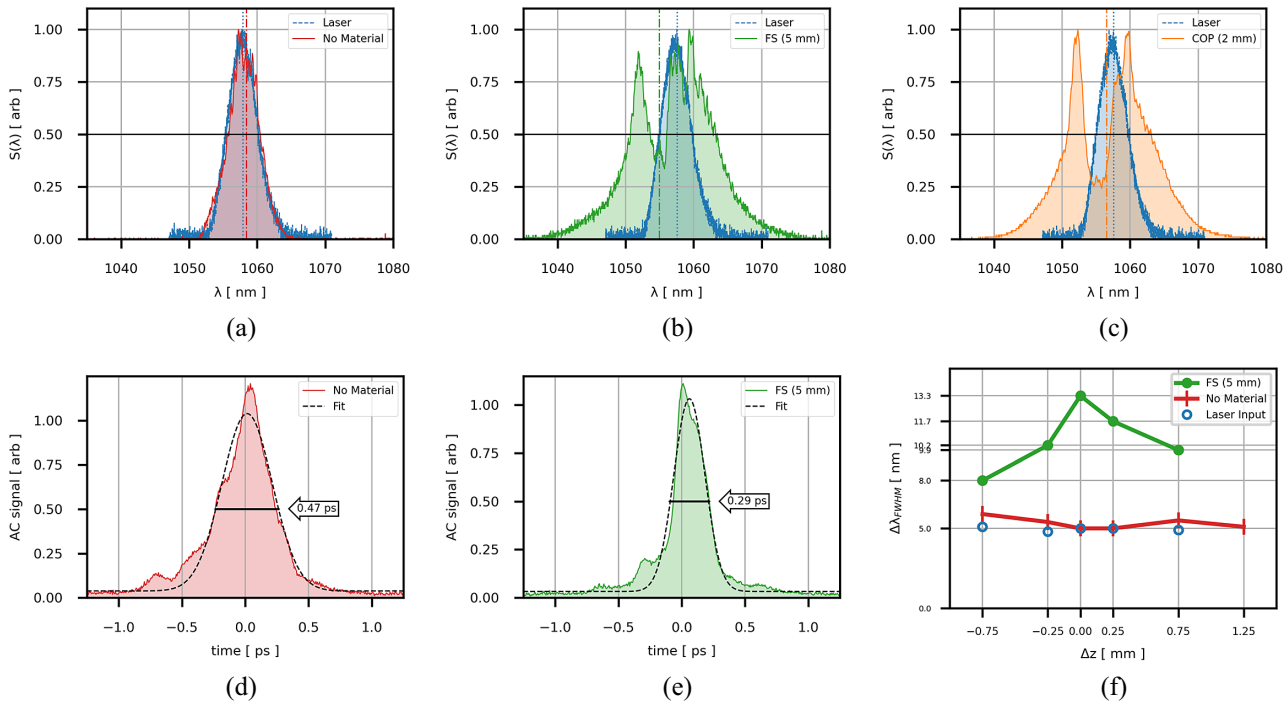

Figure 4. The spectral broadening occurring due to self-phase modulation (SPM) with no material (red line), fused silica (green line) and COP (orange line) is compared with the laser spectrum measured before the interaction (blue dashed) in (a)–(c). The initial pulse spectrum measured with no material presented in (a) shows no significant change in the spectra. In (b), a 4.8 J pulse interacts with 5 mm of fused silica, and (c) shows the result of a 3.9 J pulse passing through 2 mm of COP. The autocorrelator measurements shown in (d) and (e) give the FWHM fit in the case of no material (0.50 ± 0.05 ps) and fused silica (0.41 ± 0.9 ps), which correspond to pulse durations for the specific cases shown of 0.34 and 0.2 ps, respectively. In (f), the resulting spectral FWHM bandwidth in nm is measured relative to the input pulse chirp, as defined by the variation of the laser compressor grating separation (Δz [mm]). The initial FWHM bandwidth measured with no material (red vertical line) remains fairly constant at 5.1 nm despite the change in the separation of the laser compressor gratings. With the FS, the compressor position becomes optimized when the broadened bandwidth (green dot) is maximized relative to the measured laser bandwidth (blue circle).

contributions from the optics in the beam transport – that is, telescope lenses, vacuum window and beamsplitters – are sufficient to introduce the additional chirp of 1000 fs^2. A double pass through the mirror assembly is proposed for future applications of the system at these pulse durations.

In Figure 4(f), the dependence of the spectral FWHM bandwidth with FS is compared with no material as a function of the chirp of the input pulse by varying the separation of the gratings in the laser compressor.

With the FS installed, the optimized compressor position was retrieved when the bandwidth was maximized at 13.3 nm and then decreased as the grating separation moved in either direction.

3.3. Beam spatial profile

In Figure 5, full aperture images of the beam from the BP2 diagnostics, before (Figure 5(a)) and after (Figure 5(b)) the material insertion, illustrate the evolution of the spatial modulation. Two circular regions are selected for the spatial frequency analysis of the modulations in the beam. The region labeled I in Figure 5(a) corresponds to high average fluence, while the region labeled II has 1.7 times less, corresponding to the reduced B-integral.

In Figure 5(c), the angular integration of the 2D fast Fourier transform (FFT) of the two beam profile regions before and after the introduction of the materials quantifies the small-scale spatial features that develop within the beam profile due to the SPM.

The near-field system is capable of resolving images with the smallest feature of the beam of approximately 0.59 mm ($q \sim 1.7$ mm^{-1}) due to the size of the pixels relative to the image of the beam.

Figure 5(d) depicts the ratio of the power spectra before and after the introduction of the nonlinear material, for each of the two regions. Several features are observed: the relative gain at high frequencies of approximately 4 stays flat in the spatial modulation instabilities over the accessible frequencies for both curves, even though there is a 1.7 factor difference in the B-integral.

However, at low spatial frequencies the behavior is different. The low-intensity region II has reduced the gain of the modulations below 0.3 mm^{-1}, while the high-intensity region indicates gain in the modulation for the region 0.1–0.3 mm^{-1}.

This is the signature of the presence of two types of self-focusing: large-scale and SSSF. Large-scale self-focusing is determined by P_{cr} and if the length of the medium is close to the length of self-focusing, one can observe it.

https://doi.org/10.1017/hpl.2023.10 Published online by Cambridge University Press

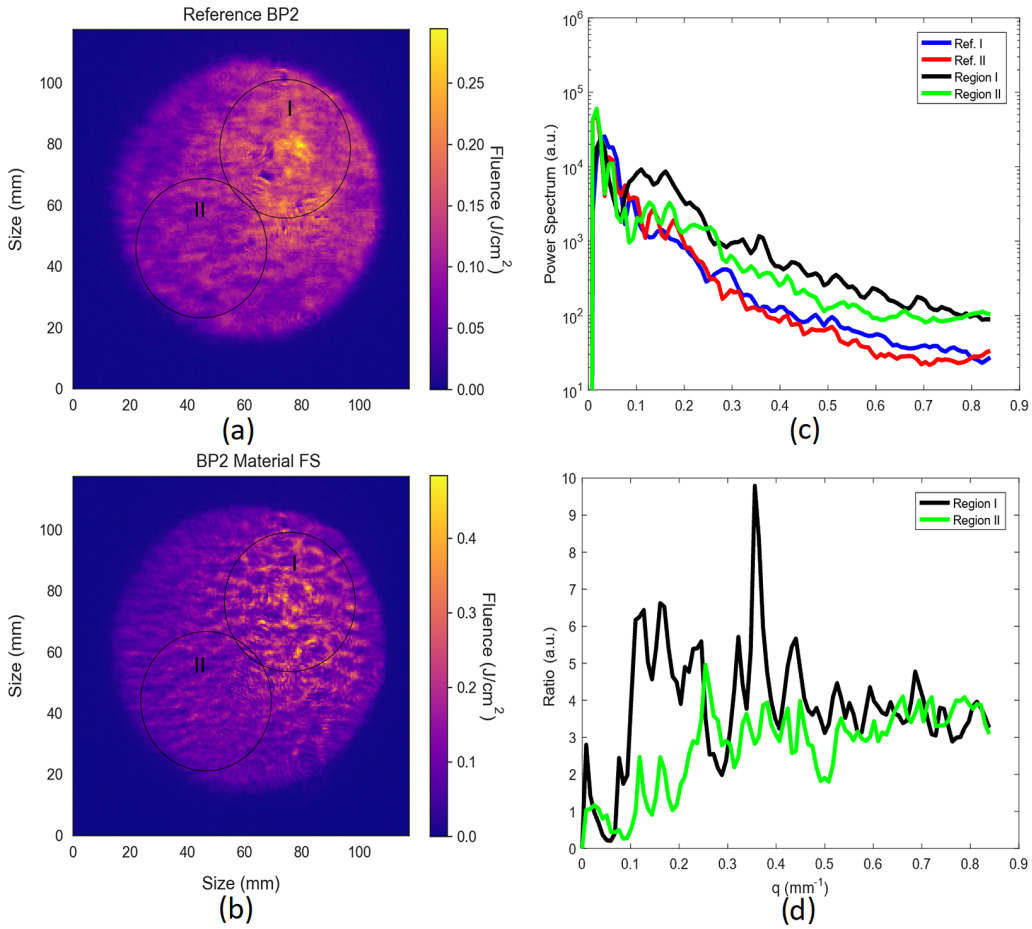

Figure 5. Beam profile comparison between the reference (a) and FS (b); in (c) the power spectrum of two separate laser regions (regions I and II, denoted by black and green, respectively), before and after the nonlinear interaction. The ratio of the power spectra, relative to the initial corresponding reference, gives the relative gain in the spatial modulation instabilities (SMIs) in (d).

The growth amplitude of the spatial harmonics starts to be observable when the B-integral becomes larger than unity and its frequencies belong to an amplification band. The boundary of the band depends on the beam intensity and cubic nonlinearity coefficient n_2, and does not depend on the length of the nonlinear plate (see, for example, Ref. [40]).

A similar behavior of the spatial noise amplification was observed in Ref. [41] (Figure 4, where $L = 200$ mm has similar pattern to our beam profile), where the gain factor of spatial noise depends on the spatial frequency and B-integral. A simple theoretical model, which describes a monochromatic plane wave instability in media with cubic nonlinearity, has been demonstrated (see Ref. [40] and references therein). This model indicates that the position of maxima and dips, in the dependence of the spatial noise amplification gain factor versus spatial frequency, is determined by a B-integral value and the distance between the spatial noise source and the nonlinear sample. In real laser setups, sources of spatial noises are distributed along the beam path and the behavior of the gain factor versus spatial frequencies, which can be observed in experiments, is not well described by the model and requires additional studies. Moreover, there are at least two factors that need to be taken into account in the theoretical model: spatial[42,43] and temporal filtering of spatial harmonics from an area of strong field inside a nonlinear sample. Both lead to an additional suppression of SSSF developments.

Analysis of an amplification of spatial harmonic amplitudes is useful in order to estimate the amount of B-integral and to limit the amplification of SSSF at the value when it becomes detrimental to the quality of the beam.

4. Conclusion

A proof-of-principle demonstration was presented of the post-compression for long pulses (> 100 fs) with multi-Joule input energies. The spectral broadening of a 350 fs pulse in FS is measured to increase from 5.0 to 13.3 nm and is capable of supporting a pulse as short as 124 fs. Following energy attenuation and a set of CMs, sufficient phase correction provides a measured reduction in pulse duration to 200 fs. When using large-aperture CMs, no energy attenuation would be required; hence, the peak intensity of the propagating pulse

https://doi.org/10.1017/hpl.2023.10 Published online by Cambridge University Press

can be enhanced from 0.23 to 0.37 TW/cm^2, under the measured, partially compensated pulse duration. With further optimization, this could lead to a peak intensity of 0.6 TW/cm^2 in the case of the shortest pulse of 124 fs. A second TFC stage could then even further compress the pulse in the future[10]. In such a case, multiple large-aperture CMs could be used after the first spectral broadening stage, and the focusability of the pulse remains correctable when sufficient quality optical films are employed.

The experimental and theoretical predictions retrieved from Ref. [41] are qualitatively and quantitatively reproduced by the results obtained at ELFIE. Hence, the experiment at ELFIE complements and partly confirms the theoretical predictions.

Despite the shot-to-shot fluctuations coupled with the low repetition rate of the laser system, which made the optimization of the pulse duration signal difficult, the post-compression method proves simple to implement within a laser system and under consistent conditions should remain robust. The development of large-aperture negative-dispersive mirrors will make the inclusion of such a post-compressor possible for full energy delivery to the target. For an existing facility, the need to effectively transport the modified pulse requires considering the bandwidth limitations in the coatings or additional contribution to the dispersion due to the subsequent optics in the beamline. However, the compactness of the TFC offers flexibility of its placement within the beam transport.

Acknowledgements

This work was supported by the Center of Excellence 'Center of Photonics', Ministry of Science and Higher Education of the Russian Federation (contract No. 075-15-2020-906), Project ELI-RO 16/2020 SBUF funded by the Institute for Atomic Physics (IFA) and by the Council for Doctoral Studies (CSUD), University of Bucharest.

References

1. J. A. Wheeler, G. Mourou, and T. Tajima, Rev. Accel. Sci. Technol. **10**, 227 (2019).
2. D. Strickland and G. Mourou, Opt. Commun. **56**, 219 (1985).
3. D. Strickland, Rev. Mod. Phys. **91**, 030502 (2019).
4. G. Mourou, Rev. Mod. Phys. **91**, 030501 (2019).
5. C. Markos, J. C. Travers, A. Abdolvand, B. J. Eggleton, and O. Bang, Rev. Mod. Phys. **89**, 045003 (2017).
6. T. Nagy, P. Simon, and L. Veisz, Adv. Phys. **6**, 1845795 (2020).
7. M. Hanna, F. Guichard, N. Daher, Q. Bournet, X. Delen, and P. Georges, Laser Photonics Rev. **15**, 2100220 (2021).
8. E. A. Khazanov, Quantum Electron. **52**, 208 (2022).
9. V. Chvykov, C. Radier, G. Chériaux, G. Kalinchenko, V. Yanovsky, and G. Mourou, in *Conference on Lasers and Electro-Optics 2010* (OSA, 2010), paper JThG4.
10. G. Mourou, S. Mironov, E. Khazanov, and A. Sergeev, Eur. Phys. J. Spec. Top. **223**, 1181 (2014).
11. E. A. Khazanov, S. Y. Mironov, and G. Mourou, Uspekhi Fizicheskih Nauk **189**, 1173 (2019).
12. V. N. Ginzburg, I. V Yakovlev, A. S. Zuev, A. P. Korobeynikova, A. A. Kochetkov, A. A. Kuzmin, S. Y. Mironov, A. A. Shaykin, I. A. Shaikin, and E. A. Khazanov, Quantum Electron. **50**, 331 (2020).
13. S. Y. Mironov, J. Wheeler, R. Gonin, G. Cojocaru, R. Ungureanu, R. Banici, M. Serbanescu, R. Dabu, G. Mourou, and E. A. Khazanov, Quantum Electron. **47**, 173 (2017).
14. S. Y. Mironov, V. N. Ginzburg, I. V Yakovlev, A. A. Kochetkov, A. A. Shaykin, E. A. Khazanov, and G. A. Mourou, Quantum Electron. **47**, 614 (2017).
15. V. N. Ginzburg, I. V Yakovlev, A. S. Zuev, A. P. Korobeynikova, A. A. Kochetkov, A. A. Kuz'min, S. Y. Mironov, A. A. Shaykin, I. A. Shaykin, and E. A. Khazanov, Quantum Electron. **49**, 299 (2019).
16. D. M. Farinella, M. Stanfield, N. Beier, T. Nguyen, S. Hakimi, T. Tajima, F. Dollar, J. Wheeler, and G. Mourou, Int. J. Mod. Phys. A **34**, 1943015 (2019).
17. D. Ursescu, D. Matei, M. Talposi, V. Iancu, V. Aleksandrov, G. Bleotu, A. Naziru, O. Tesileanu, M. Rosu, Y. Nakamiya, M. Cernaianu, B. de Boisdeffre, C. Ene, M. Caragea, A. Lazar, M. Kiss, M. Masruri, L. Caratas, A. Toader, D. Nistor, V. Luta, B. Tatulea, D. Popa, N. Stan, T. Jitsuno, R. Banici, A. Baleanu, A. Gradinariu, J. Wheeler, G. Mourou, and I. Dancus, in *Frontiers in Optics and Laser Science* (OSA, 2020), paper LW5G.4.
18. S. Y. Mironov, S. Fourmaux, P. Lassonde, V. N. Ginzburg, S. Payeur, J.-C. Kieffer, E. A. Khazanov, and G. Mourou, Appl. Phys. Lett. **116**, 241101 (2020).
19. J. I. Kim, Y. G. Kim, J. M. Yang, J. W. Yoon, J. H. Sung, S. K. Lee, and C. H. Nam, Opt. Express **30**, 8734 (2022).
20. V. Ginzburg, I. Yakovlev, A. Zuev, A. Korobeynikova, A. Kochetkov, A. Kuzmin, S. Mironov, A. Shaykin, I. Shaikin, E. Khazanov, and G. Mourou, Phys. Rev. A **101**, 013829 (2020).
21. A. Shaykin, V. Ginzburg, I. Yakovlev, A. Kochetkov, A. Kuzmin, S. Mironov, I. Shaikin, S. Stukachev, V. Lozhkarev, A. Prokhorov, and E. Khazanov, High Power Laser Sci. Eng. **9**, e54 (2021).
22. S. Fourmaux, P. Lassonde, S. Y. Mironov, E. Hallin, F. Légaré, S. Maclean, E. A. Khazanov, G. Mourou, and J. C. Kieffer, Opt. Lett. **47**, 3163 (2022).
23. V. Ginzburg, I. Yakovlev, A. Kochetkov, A. Kuzmin, S. Mironov, I. Shaikin, A. Shaykin, and E. Khazanov, Opt. Express **29**, 28297 (2021).
24. P.-G. Bleotu, J. Wheeler, D. Papadopoulos, M. Chabanis, J. Prudent, M. Frotin, L. Martin, N. Lebas, A. Freneaux, A. Beluze, F. Mathieu, P. Audebert, D. Ursescu, J. Fuchs, and G. Mourou, High Power Laser Sci. Eng. **10**, e9 (2022).
25. G. Fan, P. A. Carpeggiani, Z. Tao, G. Coccia, R. Safaei, E. Kaksis, A. Pugzlys, F. Légaré, B. E. Schmidt, and A. Baltuška, Opt. Lett. **46**, 896 (2021).
26. J. Schulte, T. Sartorius, J. Weitenberg, A. Vernaleken, and P. Russbueldt, Opt. Lett. **41**, 4511 (2016).
27. G. Mourou, B. Brocklesby, T. Tajima, and J. Limpert, Nat. Photonics **7**, 258 (2013).
28. J. Wheeler, G. Mourou, and T. Tajima, Rev. Accel. Sci. Technol. **9**, 151 (2016).
29. R. Soulard, M. N. Quinn, and G. Mourou, Appl. Opt. **54**, 4640 (2015).
30. I. Fsaifes, L. Daniault, S. Bellanger, M. Veinhard, J. Bourderionnet, C. Larat, E. Lallier, E. Durand, A. Brignon, and J.-C. Chanteloup, Opt. Express **28**, 20152 (2020).
31. K. Nakajima, J. Wheeler, G. Mourou, and T. Tajima, Int. J. Mod. Phys. A **34**, 1943003 (2019).
32. V. I. Bespalov and V. I. Talanov, ZhETF Pisma **3**, 471 (1966).
33. A. M. Rubenchik, S. K. Turitsyn, and M. P. Fedoruk, Opt. Express **18**, 1380 (2010).
34. A. A. Voronin and A. M. Zheltikov, Phys. Rev. A **94**, 023824 (2016).

https://doi.org/10.1017/hpl.2023.10 Published online by Cambridge University Press

35. A. A. Voronin, A. M. Zheltikov, T. Ditmire, B. Rus, and G. Korn, Opt. Commun. **291**, 299 (2013).
36. D. M. Farinella, J. Wheeler, A. E. Hussein, J. Nees, M. Stanfield, N. Beier, Y. Ma, G. Cojocaru, R. Ungureanu, M. Pittman, J. Demailly, E. Baynard, R. Fabbri, M. Masruri, R. Secareanu, A. Naziru, R. Dabu, A. Maksimchuk, K. Krushelnick, D. Ros, G. Mourou, T. Tajima, and F. Dollar, J. Opt. Soc. Am. B **36**, (2019).
37. A. J. Taylor, T. S. Clement, and G. Rodriguez, Opt. Lett. **21**, 1812 (1996).
38. J. Wheeler, G. P. Bleotu, A. Naziru, R. Fabbri, M. Masruri, R. Secareanu, D. M. Farinella, G. Cojocaru, R. Ungureanu, E. Baynard, J. Demailly, M. Pittman, R. Dabu, I. Dancus, D. Ursescu, D. Ros, T. Tajima, and G. Mourou, Photonics **9**, 715 (2022).
39. J. I. Kim, J. I. Kim, J. W. Yoon, J. W. Yoon, J. M. Yang, Y. G. Kim, J. H. Sung, J. H. Sung, S. K. Lee, S. K. Lee, S. K. Lee, C. H. Nam, C. H. Nam, and C. H. Nam, Opt. Express **30**, 26212 (2022).
40. A. K. Potemkin, E. A. Khazanov, M. A. Martyanov, and M. S. Kochetkova, IEEE J. Quantum Electron. **45**, 336 (2009).
41. V. N. Ginzburg, A. A. Kochetkov, A. K. Potemkin, and E. A. Khazanov, Quantum Electron. **48**, 325 (2018).
42. S. Y. Mironov, V. V. Lozhkarev, V. N. Ginzburg, I. V. Yakovlev, G. Luchinin, A. Shaykin, E. A. Khazanov, A. Babin, E. Novikov, S. Fadeev, A. M. Sergeev, and G. A. Mourou, IEEE J. Select. Top. Quantum Electron. **18**, 7 (2012).
43. S. Mironov, V. Lozhkarev, G. Luchinin, A. Shaykin, and E. Khazanov, Appl. Phys. B **113**, 147 (2013).

https://doi.org/10.1017/hpl.2023.10 Published online by Cambridge University Press